

Research

Facile synthesis of hierarchical $W_{18}O_{49}$ microspheres by solvothermal method and their optical absorption properties

Yuanpeng Xiong¹ · Bo Wu² · Yuanzhi Lin¹ · Mingwen Zhang¹ · Jintian Chen¹

Received: 28 December 2023 / Accepted: 6 March 2024

Published online: 17 May 2024

© The Author(s) 2024 [OPEN](#)

Abstract

In this study, a simple route for the synthesis of hierarchical $W_{18}O_{49}$ assembled by nanowires is reported. The morphologies and formation of $W_{18}O_{49}$ single-crystal could be controlled by changing the concentration of WCl_6 -ethanol solution. This synthesis strategy has the advantages that the hierarchical $W_{18}O_{49}$ microspheres could be economic synthesized at 180 °C without adding additives. Furthermore, efficient optical absorption properties in ultraviolet, visible and near-infrared region were obtained for the hierarchical $W_{18}O_{49}$ microspheres comparing with nanowires. These results will further promote the research of tungsten-based oxide nanomaterials.

Highlights

1. The hierarchical $W_{18}O_{49}$ microspheres assembled by nanowires were solvothermally synthesized at 180 °C via using tungsten chloride and ethanol as reactants and without adding morphology control agent or using expensive alcohol, such as isopropanol or acetic acid.
2. The $W_{18}O_{49}$ nanowires tend to form hierarchical microspheres with the increase of WCl_6 -ethanol solution concentration.
3. The absorbance (300–2400 nm) of hierarchical $W_{18}O_{49}$ microspheres synthesized at 180 °C were stronger than $W_{18}O_{49}$ nanowires synthesized at 200 °C.

Keywords Hierarchical structure · Nanowire · Optical absorption · Solvothermal synthesis · $W_{18}O_{49}$

1 Introduction

The synthesis of hierarchical structure assembled by low-dimensional nanostructures is a prerequisite for realizing the application of nanomaterials. The chemical and physical properties of hierarchical structures, as well as their applications, highly depend on their size, shape, and assembly of nanostructures [1, 2]. Many methods have been reported for the synthesis of hierarchical structures [3, 4]. However, it still remains a challenge to develop a facile, surfactant/stabilizer-free, economic synthesis strategy for the formation of hierarchical nanostructures.

✉ Yuanpeng Xiong, xiongpeng@163.com | ¹School of Materials and Package Engineering, Fujian Polytechnic Normal University, Fuqing 350300, China. ²School of Materials Science and Engineering, Fuzhou University, Fuzhou 350108, China.



Tungsten oxides-based nanostructure has been employed for a wide variety of applications due to its unique structure, such as gas sensors [5–8], electro-catalytic [9]. $W_{18}O_{49}$ is a kind of substoichiometric compounds, which contains tungsten ions of mixed valences along with the largest oxygen vacancy among the substoichiometric composition of tungsten oxide. The synthesis of $W_{18}O_{49}$ is of great interest due to its unusual structure. Nano- $W_{18}O_{49}$ has been found to have excellent optical absorption properties in near-infrared region [10–14]. The most common methods for the synthesis of hierarchical $W_{18}O_{49}$ nanostructures reported are limited to high temperature [15], using inorganic additives [16, 17], using expensive solvents, such as CH_3COOH [18] or isopropanol [19].

Herein, we report a simple route for the synthesis of hierarchical $W_{18}O_{49}$ microspheres assembled by nanowires. The hierarchical $W_{18}O_{49}$ were solvothermally synthesized at 180 °C using WCl_6 and ethanol, and without adding morphology control agent.

2 Experiment

2.1 Materials

Tungsten chloride (99%) was purchased from Aladdin Co. Ltd. Ethanol was purchased from Beijing Chemical Co. Ltd. All reagents were analytical and used without further purification.

2.2 Synthesis of $W_{18}O_{49}$

A certain amount of tungsten chloride was dissolved in 20 mL ethanol. Then, the volume of above solution was adjusted to 25 mL. The obtained solution was transferred into Teflon-lined autoclave of 50 mL internal volume, followed by solvothermal reaction in an electric oven under a certain temperature for 24 h. After the reaction, the obtained powder was centrifuged, washed 4 times with water and ethanol, and dried in a drying oven at 60 °C.

2.3 Characterization

The phase of samples was determined by X-ray diffraction (XRD, Rigaku D/max 2200 PC) using graphite monochromatized Cu K α . The morphology and microstructure of samples were observed by scanning electron microscopy (SEM, JSM 7500F) and transmission electron microscopy (TEM, JEM-2100F).

2.4 Optical test

The optical absorption properties were investigated by an ultraviolet–visible near-infrared spectrophotometer (UV–Vis–NIR, UV-3600) using $BaSO_4$ as reference and equipped with integrating sphere. For UV–Vis–NIR, firstly, the absorbance of highly purified $BaSO_4$ powder was used as baseline. Secondly, as-synthesized powder should be stuck to the surface of a sample stage, scraped and blown to form a layer as thin as possible, and its absorbance were tested via using the absorbance of $BaSO_4$ powder as baseline.

The band gap (E_g) of as-synthesized powder was calculated by employing their UV–Vis–NIR absorption spectra. The energy-dependent absorption coefficient α in the vicinity of the absorption edge can be expressed as Eq. (1) [15, 20, 21]:

$$\alpha h\nu = B(h\nu - E_g)^n \quad (1)$$

where B is a constant related the materials, $h\nu$ is the incident photon energy, n depends on the kind of optical transitions. Specifically, n is 1/2 and 2 for transition being direct allowed and indirect allowed, respectively.

In accordance with Lambert–Beer’s law [21]:

$$A = \alpha bc$$

where A is absorbance, b and c are constants related the testing condition. For the samples, the value of b and c is certain. So, the equation can be described as $\alpha = A/bc = A/K$. The eq. (1) can be given as follows:

$$\frac{Ah\nu}{KB} = (h\nu - E_g)^n \quad (2)$$

3 Results and discussion

3.1 XRD analysis

Figure 1 shows the XRD patterns of samples synthesized with different WCl_6 -ethanol concentration at 180 °C. The diffraction peaks were similar with current reported literature [7]. All diffraction peaks were indexed to the monoclinic $\text{W}_{18}\text{O}_{49}$ (JCPDS No. 71-2450), and no impurity peaks were identified. It could be seen the (010) and (020) plane had the sharp diffraction peaks for all samples. Other peaks were weak and not sharp, indicating as-synthesized $\text{W}_{18}\text{O}_{49}$ tend to grow along [010] direction, which agree well with prior literature, since the close-packed planes of monoclinic $\text{W}_{18}\text{O}_{49}$ are (010) [17]. Noteworthy, the (010) and (020) peaks of samples synthesized with 0.005 mol/L and 0.01 mol/L WCl_6 -ethanol solution were slightly shift to lower angle. That is, as the WCl_6 -ethanol concentration was low, the mole fraction of oxygen vacancy in $\text{W}_{18}\text{O}_{49}$ was low because the ethanol is a source of oxygen in this route. The sample synthesized with 0.005 mol/L WCl_6 -ethanol solution had the lowest diffraction intensity, indicating it has the lowest crystallinity. As the WCl_6 -ethanol concentration was 0.02 mol/L, the diffraction peaks were matched well with standard card. The color of these samples was blue, which may originate from the chromophore of W^{5+} [22].

To further investigate the effect of reaction temperature on the phase, Fig. 2 shows the XRD patterns of samples synthesized with different WCl_6 -ethanol concentration at 200 °C. Comparing with those synthesized at 180 °C, the phase of as-synthesized samples was similar. All samples diffraction peaks matched well with the standard card. All other peaks were weaker and not sharp except (010) and (020) peaks, indicating as-synthesized $\text{W}_{18}\text{O}_{49}$ tend to grow along [010] direction. This was similar with those synthesized at 180 °C. The sample synthesized with 0.02 mol/L WCl_6 -ethanol solution had the strongest diffraction intensity, indicating it has highest crystallinity. More remarkably, the color of these samples was deeper blue than those synthesized at 180 °C, this may be related to the higher reduction ability of ethanol derived from higher reaction temperature.

3.2 Morphology analysis

Figure 3 shows the SEM images of $\text{W}_{18}\text{O}_{49}$ synthesized with different WCl_6 -ethanol concentration at 180 °C. It could be seen the $\text{W}_{18}\text{O}_{49}$ synthesized via 0.005 mol/L WCl_6 -ethanol solution were consisted by nanowires (Fig. 3a). The length of nanowires exceeds 1 μm . As the WCl_6 -ethanol concentration was 0.01 mol/L, the $\text{W}_{18}\text{O}_{49}$ nanowires aggregate apparently (Fig. 3b). Some nanowires form a tightly bonded irregularity structure. As the concentration of WCl_6 -ethanol solution was 0.02 mol/L, the $\text{W}_{18}\text{O}_{49}$ were consisted by hierarchical microspheres with diameter around 1–2 μm (Fig. 3c). Further

Fig. 1 The XRD patterns of samples synthesized via **a** 0.005 mol/L; **b** 0.01 mol/L; **c** 0.02 mol/L WCl_6 -ethanol solution at 180 °C

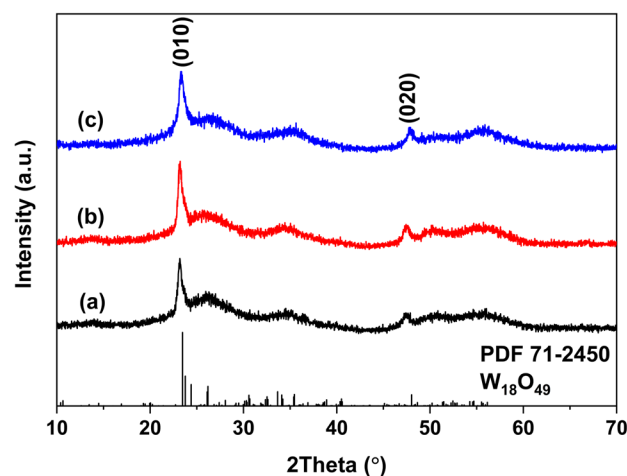


Fig. 2 The XRD patterns of samples synthesized via **a** 0.005 mol/L; **b** 0.01 mol/L; **c** 0.02 mol/L WCl_6 -ethanol solution at 200 °C

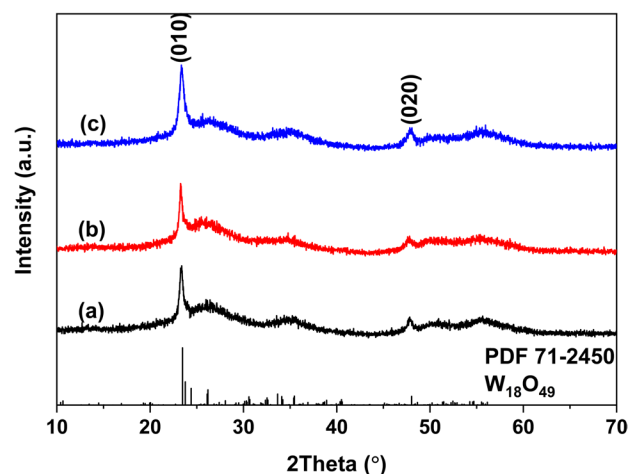
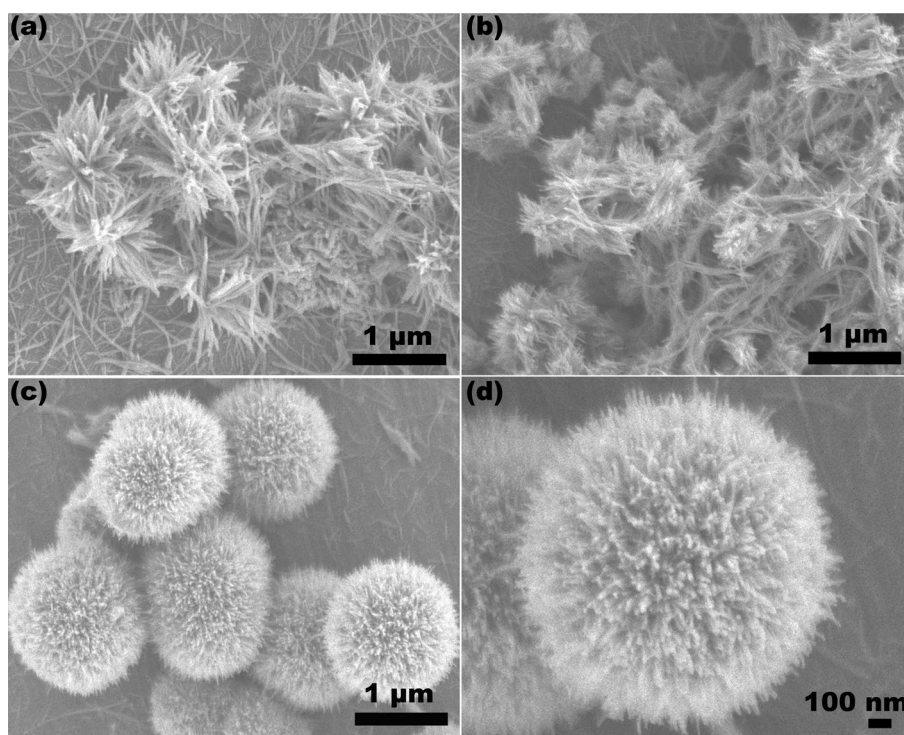


Fig. 3 The SEM images of $\text{W}_{18}\text{O}_{49}$ synthesized via **a** 0.005 mol/L; **b** 0.01 mol/L; **c, d** 0.02 mol/L WCl_6 -ethanol solution at 180 °C



magnifying the SEM observation power, it could be seen the hierarchical microspheres were assembled by nanowires (Fig. 3d).

Figure 4 shows the morphology of $\text{W}_{18}\text{O}_{49}$ synthesized with different WCl_6 -ethanol concentration at 200 °C. It could be seen the $\text{W}_{18}\text{O}_{49}$ synthesized via 0.005 mol/L WCl_6 -ethanol solution were consisted by nanofibers with diameter around 20–30 nm and length exceed 1 μm (Fig. 4a). The diameter of nanofibers was larger than those synthesized at 180 °C with similar WCl_6 -ethanol concentration, this may relate to the higher reaction temperature. As the concentration of WCl_6 -ethanol solution was 0.01 mol/L, $\text{W}_{18}\text{O}_{49}$ were consisted by some tightly bonded irregularity particles and randomly dispersed nanorods (Fig. 4b). Magnifying the SEM observation power, it was found that the irregularity particles were constructed by nanorods (Fig. 4c). Comparing with those synthesized via 0.005 mol/L WCl_6 -ethanol solution at 200 °C, the length of nanorod were decreased to 0.3–1 μm. This may relate to the high WCl_6 -ethanol solution which contributed to high supersaturation of tungsten source, prohibited the growth of $\text{W}_{18}\text{O}_{49}$ along the [010] direction [23]. Further observed by TEM, it was found that the nanorods were assembled by nanowires (Fig. 4d). The HRTEM image of this sample show clear lattice fringes. The interplanar spacing of these fringes were 0.378 nm (Fig. 4e), agree with the

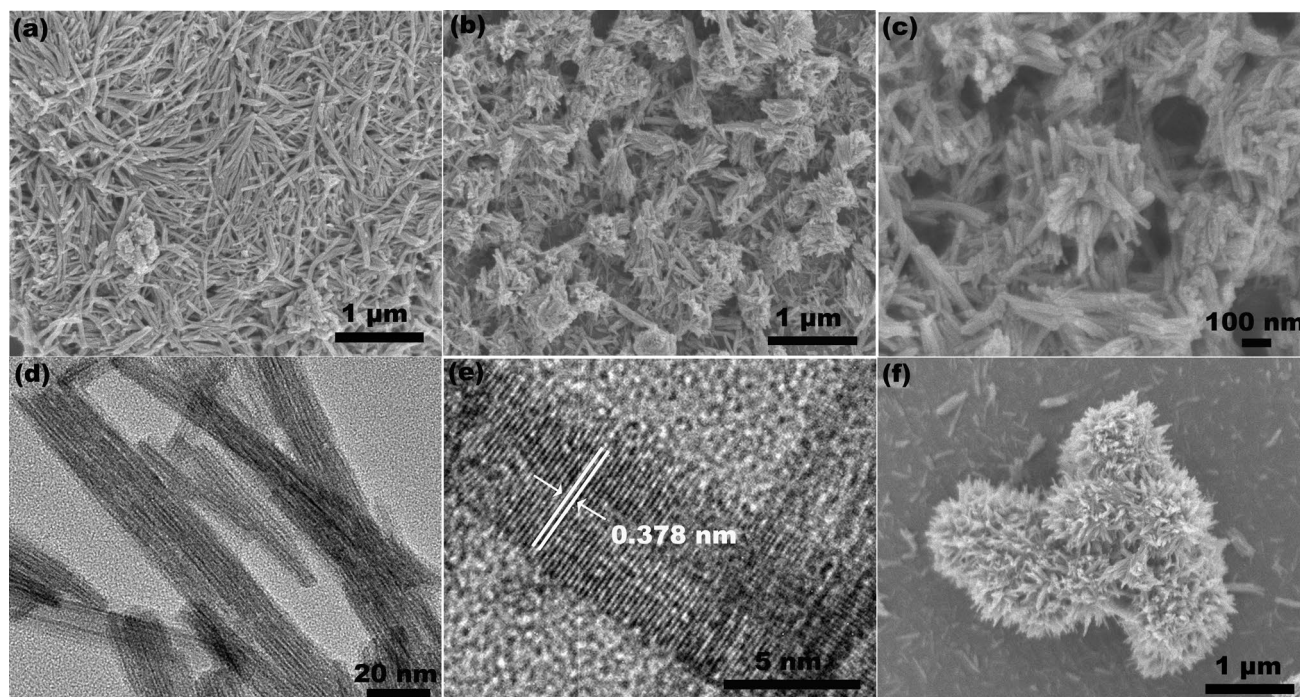


Fig. 4 **a, b, c, f** SEM images and **d, e** TEM image of $W_{18}O_{49}$ synthesized via **a** 0.005 mol/L; **b, c, d, e** 0.01 mol/L; **f** 0.02 mol/L WCl_6 -ethanol solution at 200 °C

(010) plane of the monoclinic $W_{18}O_{49}$. The TEM analytical results indicated that the $W_{18}O_{49}$ nanowires grow along [010] direction, which agree with XRD analysis. As the concentration of WCl_6 -ethanol solution was 0.02 mol/L, the morphology of $W_{18}O_{49}$ was transformed to hierarchical microspheres with diameter around 1–2 μm (Fig. 4f).

3.3 Formation mechanism

Based on above results, it could be concluded that increasing the WCl_6 -ethanol concentration was benefit for the synthesis of hierarchical $W_{18}O_{49}$ microspheres. Figure 5 depicts a probable crystal growth process via self-assembly of $W_{18}O_{49}$. It could be divided into three steps, *i.e.*, firstly, a large number of $W_{18}O_{49}$ crystal nuclei were formed under solvothermal conditions. Since the close-packed planes of monoclinic $W_{18}O_{49}$ are (010), the crystal nuclei tend to grow along [010] direction and form $W_{18}O_{49}$ nanowires [16]. Secondly, it has been reported that oxygen vacancies exposed along the [010] direction in monoclinic $W_{18}O_{49}$ [24]. It led to the as-synthesized $W_{18}O_{49}$ nanowires have a high surface energy, and tend to aggregate to lessen the surface free energy, followed by forming a tightly bonded structure. Thirdly, with the increase of WCl_6 -ethanol concentration, as well as reaction time, the size of $W_{18}O_{49}$ nanowires increased, and the water produced by the reaction among ethanol molecules decreased, following the decrease of hydrogen bond. It led to the decrease

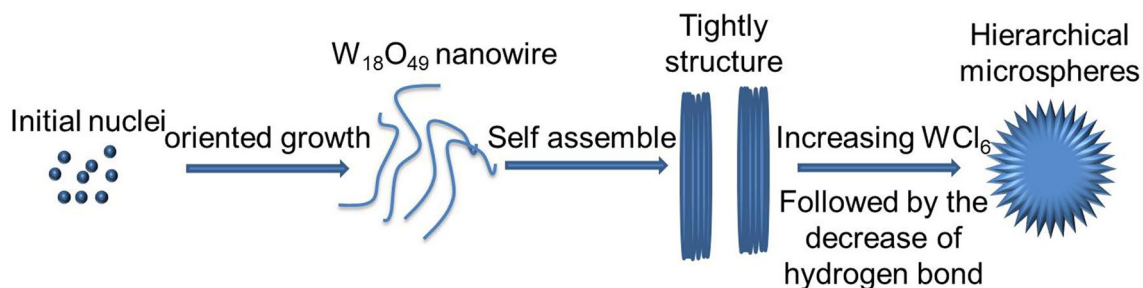


Fig. 5 Schematic of the self-assembly processes to give a hierarchical structure of $W_{18}O_{49}$

Fig. 6 The UV–Vis–NIR spectra of **a** $W_{18}O_{49}$ hierarchical microspheres synthesized via 0.02 mol/L WCl_6 -ethanol solution at 180 °C; **b** $W_{18}O_{49}$ nanowires synthesized via 0.01 mol/L WCl_6 -ethanol solution at 200 °C

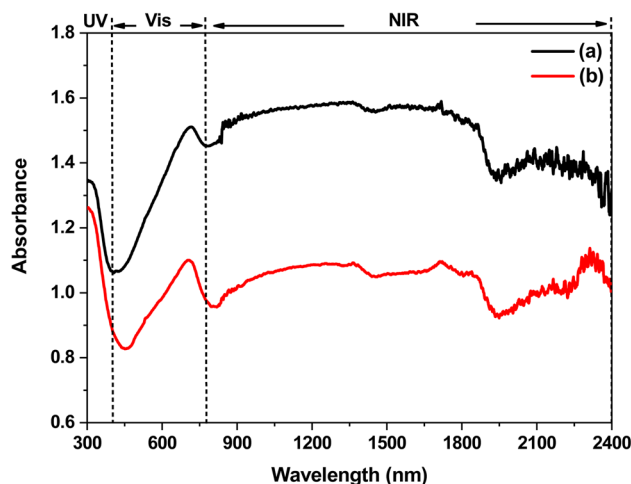
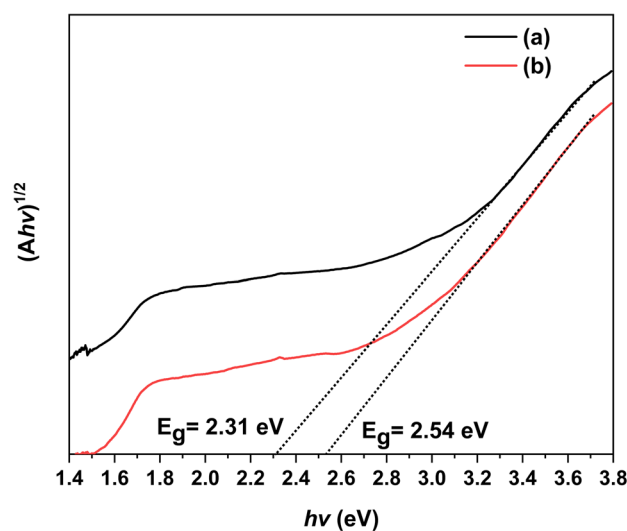


Fig. 7 The band gap (E_g) of **a** $W_{18}O_{49}$ hierarchical microspheres synthesized via 0.02 mol/L WCl_6 -ethanol solution at 180 °C; **b** $W_{18}O_{49}$ nanowires synthesized via 0.01 mol/L WCl_6 -ethanol solution at 200 °C calculated based on an indirect allowed transition ($(Ah\nu)^{1/2}$ vs. $h\nu$)



of surface energy for the $W_{18}O_{49}$ nanowires, and weaken the bonding force among $W_{18}O_{49}$ nanowires. As a result, the tightly structure was transformed to hierarchical microspheres.

3.4 Evaluation of optical absorption property

To investigate the optical absorption properties of as-synthesized $W_{18}O_{49}$ samples, Fig. 6 shows the UV–Vis–NIR spectra of $W_{18}O_{49}$ samples. In the region of 300–780 nm, it could be seen the absorbance of $W_{18}O_{49}$ hierarchical microspheres synthesized via 0.02 mol/L WCl_6 -ethanol solution at 180 °C was stronger than $W_{18}O_{49}$ nanowires synthesized via 0.01 mol/L WCl_6 -ethanol solution at 200 °C. The minimum absorbance for these samples occurs at about 450 nm (visible light region), indicating that both of them have a certain transmittance to visible light, and the hierarchical $W_{18}O_{49}$ microspheres have stronger ultraviolet absorbance than nanowires. Additionally, these samples have a main absorption around 700 nm. This may arise from the collective oscillations of excess electrons due to the existence of abundant oxygen vacancies in $W_{18}O_{49}$ [25]. The absorbance of hierarchical $W_{18}O_{49}$ microspheres around 700 nm is stronger than $W_{18}O_{49}$ nanowires. This may be attributed to the hierarchical structures, which facilitate the multiple light scattering between the radical nanowires [15].

The $W_{18}O_{49}$ is an indirect semiconductor oxide [26], its absorption for ultraviolet and visible light may relate to band gap (E_g). Figure 7 shows the band gap of as-synthesized $W_{18}O_{49}$ calculated based on an indirect allowed transition ($(Ah\nu)^{1/2}$ vs. $h\nu$). It could be seen the band gap of hierarchical $W_{18}O_{49}$ microspheres is 2.31 eV, which is smaller than $W_{18}O_{49}$ nanowires ($E_g = 2.54$ eV). This may be one of the reason resulted in the hierarchical $W_{18}O_{49}$ microspheres have stronger absorbance than $W_{18}O_{49}$ nanowires at 300–780 nm.

Additionally, in this study, ethanol not only acts as solvent, but also acts as reducing agent that transform the W^{6+} ions to W^{5+} . The higher reaction temperature was benefit to induce more W^{6+} ions transform to W^{5+} , following the increase of free electron concentration. However, the testing data show opposite results in Fig. 6, indicating the morphology of above samples play important role on their optical absorption properties.

In the near infrared region (NIR, 780–2400 nm), it could be seen that both of above $W_{18}O_{49}$ samples had broad absorption spectrum, and the hierarchical $W_{18}O_{49}$ microspheres had stronger absorbance than $W_{18}O_{49}$ nanowires. The properties of the hierarchical $W_{18}O_{49}$ microspheres should be good news for those who want to understand the near-infrared absorption of hierarchical tungsten oxides-based nanostructure constructed by low-dimensional nanostructures. Now, some researchers attribute the NIR absorption mechanism of tungsten-based oxide to many theories, such as plasmon resonance of free electrons [27, 28], small polaron [29], or interband transition [30]. These theories are somehow related to quantum confinement. For the one-dimensional nanostructure, the quantum confinement leads to the continuous energy level in one dimension transform to discrete energy level, the carriers in nanostructure cannot move free in this dimension. Under the radiation of near-infrared light, electrons in this dimension can be excited to high level, following the absorption of light. However, in the matter of hierarchical $W_{18}O_{49}$ structures responding to near-infrared light, how they work, is yet unknown. It was reported that the hierarchical nanostructure not only has the physical and chemical characteristics of low-dimensional nanostructures, but also can act as a mirror cavity [10], *i.e.*, the incident light enter into the cavity may be reflected many times, following the increasing number of absorption, thereby improve the NIR absorbance of hierarchical $W_{18}O_{49}$ microspheres. This may be one of the reason leads to hierarchical $W_{18}O_{49}$ microspheres have better NIR absorption. Moreover, smaller energy level spacing of hierarchical $W_{18}O_{49}$ microspheres ($E_g = 2.31$ eV) comparing with $W_{18}O_{49}$ nanowires ($E_g = 2.54$ eV) may be another reason, *i.e.*, it induces more electrons transit to higher energy level after absorbing photons, following improving of NIR absorption properties of hierarchical $W_{18}O_{49}$ microspheres [31, 32].

4 Conclusions

In summary, hierarchical $W_{18}O_{49}$ microspheres assembled by nanowires were economic synthesized using a facile route based on self-assembly mechanism without additives. The WCl_6 -ethanol concentration play important role on the formation of hierarchical $W_{18}O_{49}$ structure, *i.e.*, $W_{18}O_{49}$ nanowires tend to form hierarchical structures by self-assembly of nanowires with the increase of WCl_6 -ethanol concentration. The XRD, SEM and TEM results confirmed the samples formation. In addition, the excellent optical absorption in the range of 300–2400 nm of hierarchical $W_{18}O_{49}$ microspheres was demonstrated. The morphology and band gap have significant effects on the optical absorption properties of $W_{18}O_{49}$.

Acknowledgements This work was financially supported by the National Natural Science Foundation of China (21902026), Educational Research Project of Young and Middle-aged Teacher of Fujian Province (JAT210378), and Fujian Xinfuxing Glass Co., Ltd (HX2021086).

Author contributions Yuanpeng Xiong: Methodology, Data curation, Writing - original draft, Writing - review & editing Bo Wu: Writing - original draft, Writing - review & editing. Yuanzhi Lin: provide experimental condition. Mingwen Zhang: provide experimental condition. Jintian Chen: provide experimental condition.

Data availability Data will be made available on request.

Declarations

Competing interests The authors declare no competing interests.

Open Access This article is licensed under a Creative Commons Attribution 4.0 International License, which permits use, sharing, adaptation, distribution and reproduction in any medium or format, as long as you give appropriate credit to the original author(s) and the source, provide a link to the Creative Commons licence, and indicate if changes were made. The images or other third party material in this article are included in the article's Creative Commons licence, unless indicated otherwise in a credit line to the material. If material is not included in the article's Creative Commons licence and your intended use is not permitted by statutory regulation or exceeds the permitted use, you will need to obtain permission directly from the copyright holder. To view a copy of this licence, visit <http://creativecommons.org/licenses/by/4.0/>.

References

1. Lee JH. Gas sensors using hierarchical and hollow oxide nanostructures: overview. *Sensor Actuat B Chem.* 2009;140(1):319–36.
2. Sui LL, Wang R, Zhao D, Shen SC, Sun L, Xu YM, Cheng XL, Huo LH. Construction of hierarchical α - MoO_3 hollow microspheres and its high adsorption performance towards organic dyes. *J Inorg Mater.* 2019;34(2):193–200.
3. Wang QS, Wang H, Yang Y, Jin LH, Liu Y, Wang Y, Yan XY, Xu J, Gao RQ, Lei PP. Plasmonic Pt superstructures with boosted near-infrared absorption and photothermal conversion efficiency in the second biowindow for cancer therapy. *Adv Mater.* 2019;31(46):1904836.
4. Xiao ZY, Xu CT, Jiang XH, Zhang WL, Peng YX, Zou RJ, Huang XJ, Liu Q, Qin ZY, Hu JQ. Hydrophilic bismuth sulfur nanoflower superstructures with an improved photothermal efficiency for ablation of cancer cells. *Nano Res.* 2016;9(7):1934–47.
5. Yang XJ, Salles V, Kaneti YV, Liu MS, Maillard M, Journet C, Jiang XC, Brioude A. Fabrication of highly sensitive gas sensor based on Au functionalized WO_3 composite nanofibers by electrospinning. *Sensor Actuat B: Chem.* 2015;220:1112–9.
6. Imran M, Rashid SSAH, Sabri Y, Motta N, Tesfamichael T, Sonar P, Shafiei M. Template based sintering of WO_3 nanoparticles into porous tungsten oxide nanofibers for acetone sensing applications. *J Mater Chem C.* 2019;7(10):2961–70.
7. Chen KY, Xie WH, Deng Y, Han JT, Zhu YH, Sun JG, Yuan KP, Wu LM, Deng YH. Alkaloid precipitant reaction inspired controllable synthesis of mesoporous tungsten oxide spheres for biomarker sensing. *ACS Nano.* 2023;17(16):15763–75.
8. Septiani NLW, Shukri G, Saputro AG, Nugraha Karim MR, Al-Mubaddel F, Hardiansyah A, Yamauchi Y, Kaneti YV. Palm sugar-induced formation of hexagonal tungsten oxide with nanorod-assembled three-dimensional hierarchical frameworks for nitrogen dioxide sensing. *ACS Sustain Chem Eng.* 2022;10(46):15035–45.
9. Ahmed J, Alhokbany N, Ahamad T, Alsheri SM. Investigation of enhanced electro-catalytic HER/OER performances of copper tungsten oxide@reduced graphene oxide nanocomposites in alkaline and acidic media. *New J Chem.* 2022;46:1267–72.
10. Tian QW, Tang MH, Sun YG, Zou RJ, Chen ZG, Zhu MF, Yang SP, Wang JL, Wang JH, Hu JQ. Hydrophilic flower-like CuS superstructures as an efficient 980 nm laser-driven photothermal agent for ablation of cancer cells. *Adv Mater.* 2011;23(31):3542–7.
11. Takeda H, Adachi K. Near infrared absorption of tungsten oxide nanoparticle dispersion. *J Am Ceram Soc.* 2007;90(12):4059–61.
12. Guo CS, Yin S, Yan M, Kobayashi M, Kakihana M, Sato T. Morphology-controlled synthesis of $\text{W}_{18}\text{O}_{49}$ nanostructures and their near-infrared absorption properties. *Inorg Chem.* 2012;51(8):4763–71.
13. Guo CS, Yin S, Dong Q, Sato T. The near infrared absorption properties of $\text{W}_{18}\text{O}_{49}$. *RSC Adv.* 2012;2(12):5041–3.
14. Li GL, Wu G, Guo CS, Wang BS. Fabrication of one-dimensional $\text{W}_{18}\text{O}_{49}$ nanomaterial for the near infrared shielding. *Mater Lett.* 2016;169:227–30.
15. Wang J, Wang ZX, Gao JC, Ye J. Study on the photocatalytic properties differences between the 1-D and 3-D $\text{W}_{18}\text{O}_{49}$ particles. *RSC Adv.* 2023;13(16):10657–66.
16. Li B, Zhang YX, Zou RJ, Wang Q, Zhang BJ, An L, Yin F, Hua YQ, Hu JQ. Self-assembled WO_{3-x} hierarchical nanostructures for photothermal therapy with a 915 nm laser rather than the common 980 nm laser. *Dalton T.* 2014;43(16):6244–50.
17. Shirke YM, Mukherjee SP. Selective synthesis of WO_3 and $\text{W}_{18}\text{O}_{49}$ nanostructures: ligand-free pH-dependent morphology-controlled self-assembly of hierarchical architectures from 1D nanostructure and sunlight-driven photocatalytic degradation. *CrystEngComm.* 2017;19(15):2096–105.
18. Xu YS, Ma TT, Zheng LL, Zhao YQ, Liu XH, Zhang J. Heterostructures of hematite-sensitized $\text{W}_{18}\text{O}_{49}$ hollow spheres for improved acetone detection with ultralow detection limit. *Sensor Actuat B Chem.* 2019;288:432–41.
19. Hai GJ, Huang JF, Cao LY, Jie YN, Li JY, Wang X. Shape evolution of hierarchical $\text{W}_{18}\text{O}_{49}$ nanostructures: a systematic investigation of the growth mechanism, properties and morphology-dependent photocatalytic activities. *Nanomaterials.* 2016;6(12):240.
20. Gao T, Jelle BP. Visible-Light-Driven photochromism of hexagonal sodium tungsten bronze nanorods. *J Phy Chem C.* 2013;117(26):13753–61.
21. Hai GJ, Huang JF, Cao LY, Jie YN, Li JY, Wang X, Zhang G. Influence of oxygen deficiency on the synthesis of tungsten oxide and the photocatalytic activity for the removal of organic dye. *J Alloy Compd.* 2017;690:239–48.
22. Bange K. Coloration of tungsten oxide films: a model for optically active coatings. *Sol Energy Mat Sol C.* 1999;58(1):1–131.
23. Choi HG, Jung YH, Kim DK. Solvothermal synthesis of tungsten oxide nanorod/nanowire/nanosheet. *J Am Ceram Soc.* 2005;88(6):1684–6.
24. Zhou H, Shi Y, Dong QS, Lin J, Wang AQ, Ma TL. Surface oxygen vacancy-dependent electrocatalytic activity of $\text{W}_{18}\text{O}_{49}$ nanowires. *J Phy Chem C.* 2014;118(35):20100–6.
25. Liu Y, Zhang ZY, Fang YR, Liu BK, Huang JD, Miao FJ, Bao Y, Dong B. IR-driven strong plasmonic-coupling on Ag nanorices/ $\text{W}_{18}\text{O}_{49}$ nanowires heterostructures for photo/thermal synergistic enhancement of H_2 evolution from ammonia borane. *Appl Catal B: Environ.* 2019;252:164–73.
26. Liu WJ, Jiang PG, Xiao YY, Liu JS. A study of the hydrogen adsorption mechanism of $\text{W}_{18}\text{O}_{49}$ using first-principles. *Com Mater Sci.* 2018;154:53–9.
27. Lynch DW, Rosei R, Weaver JH, Olson CG. The optical properties of some alkali metal tungsten bronzes from 0.1 to 38 eV. *J Solid State Chem.* 1973;8(3):242–52.
28. Wu XY, Li Y, Zhang GK, Chen H, Li J, Wang K, Pan Y, Zhao Y, Sun YF, Xie Y. Photocatalytic CO_2 conversion of $\text{M}_{0.33}\text{WO}_3$ directly from the air with high selectivity: insight into full spectrum-induced reaction mechanism. *J Am Ceram Soc.* 2019;141(13):5267–74.
29. Schirmer OF, Wittwer V, Baur G, Brandt G. Dependence of WO_3 electrochromic absorption on crystallinity. *J Electrochem Soc.* 1977;124(5):749–53.
30. Green M, Travlos A. Sodium-tungsten bronze thin films: I. Optical properties of dilute bronzes. *Philos Mag B.* 1985;51(5):501–20.
31. Liu GH, Kong FD, Xu J, Li RX. Novel synthesis of 0D, 1D and 2D nano- Cs_xWO_3 and their tunable optical-thermal response performance. *J Mater Chem C.* 2020;8(30):10342–51.
32. Wang TY, Xiong YP, Li RX, Cai HN. Dependence of infrared absorption properties on the Mo doping contents in M_xWO_3 with various alkali metals. *New J Chem.* 2016;40(9):7476–81.